Spectral properties of a hole coupled to optical phonons in the generalized *t-J* model

J. Bonča,[1,2] S. Maekawa,[3,4] T. Tohyama,[5] and P. Prelovšek[1,2]
[1]*Faculty of Mathematics and Physics, University of Ljubljana, Ljubljana 1000, Slovenia*
[2]*J. Stefan Institute, Ljubljana 1000, Slovenia*
[3]*Institute for Materials Research, Tohoku University, Sendai 980-8577, Japan*
[4]*CREST, Japan Science and Technology Agency (JST), Kawaguchi, Saitama 332-0012, Japan*
[5]*Yukawa Institute for Theoretical Physics, Kyoto University, Kyoto 606-8502, Japan*
(Received 16 November 2007; published 28 February 2008)

We present an efficient numerical method for the description of ground state and spectral properties of a doped hole in generalized *t-J* models coupled to optical phonons. In the weak-coupling regime, coherent hole motion is less affected by the electron-phonon (EP) interaction in the electron than in the hole-doped system. Increasing the strength of EP coupling leads to a vanishing low-energy spectral weight around Γ point. Spectral properties are in the strong coupling regime consistent with recent high-resolution angle resolved photoemission spectra (ARPES) [K. M. Shen *et al.*, Phys. Rev. Lett. **93**, 267002 (2004)]. A waterfall-like feature appears connecting the dispersive low-energy band with the incoherent high-energy peak resembling ARPES data [F. Ronning *et al.*, Phys. Rev. B **71**, 094518 (2005)].

DOI: 10.1103/PhysRevB.77.054519 PACS number(s): 74.25.Jb, 71.10.Pm, 71.38.−k, 79.60.−i

I. INTRODUCTION

A description of a hole (charge carrier) motion in a strongly correlated system coupled to additional bosonic degrees of freedom represents one of the persistent open problems in the area of correlated electron systems. The accurate solution of this problem may provide crucial understanding of the interplay between strong correlations, magnetic and lattice degrees of freedom revealing the true nature of the mechanism of high-T_c superconductivity.

Current interest in this field is in part focused on the influence of the electron-phonon (EP) interaction on correlated motion of a hole in the antiferromagnetic (AFM) background.[3–5] This interest is primarily fuelled by increasing evidence given by recent angle resolved photoemission spectra (ARPES) data demonstrating that strong EP interaction plays an important role in low-energy physics of high-T_c materials.[5–10] While interplay between spin and lattice degrees of freedom seems to be in one of the focal points of research in correlated systems, there is a lack of reliable analytical as well as numerical methods. Among the most reliable is the diagrammatic Monte Carlo (DMC) method,[4] which however, treats interaction of the hole with spin degrees of freedom in the noncrossing approximation while EP interaction is treated exactly numerically. More accurate calculations at finite doping are possible also within the adiabatic approximation for lattice deformations.[11,12] Recently, dynamical mean-field calculations have been applied to the Hubbard-Holstein model away from half-filling.[13,14]

The main goals of this paper are (a) to generalize recently developed method[15] for computing static and dynamic properties of the *spin-lattice polaron* in the *t-J*-Holstein (TJH) and related models, (b) to investigate the interplay of spin and lattice degrees of freedom on quasiparticle (QP) properties, and (c) to clarify the crossover from spin polaron to small polaron by making use of the difference of hole and electron carrier in the *t-t′-t″-J* model. We also want to test the following assumptions: a) can strong EP interaction explain unusual ARPES data, as suggested in Refs. 1 and 4, and (b) can EP coupling provide a mechanism for disappearance of the spectral weight near Γ point and give rise to anomalous high-energy dispersion recently seen in insulating cuprate $Ca_2CuO_2Cl_2$.[2]

II. MODEL AND NUMERICAL METHOD

We start by writing the generalized *t-J*-Holstein model on a square lattice as

$$H = -\sum_{\mathbf{i},\mathbf{j},s} t_{\mathbf{ij}} \tilde{c}^{\dagger}_{\mathbf{i},s} \tilde{c}_{\mathbf{j},s} + J \sum_{\langle \mathbf{i},\mathbf{j} \rangle} \mathbf{S_i S_j} + g \sum_{\mathbf{i}} (1 - n_{\mathbf{i}})(a^{+}_{\mathbf{i}} + a_{\mathbf{i}}) + \omega_0 \sum_{\mathbf{i}} a^{+}_{\mathbf{i}} a_{\mathbf{i}}, \quad (1)$$

where $\tilde{c}_{\mathbf{i},s} = c_{\mathbf{i},s}(1 - n_{\mathbf{i},-s})$ is a fermion operator, projected onto a space of no double occupancy, $t_{\mathbf{ij}}$ represent nearest- ($t_{\mathbf{ij}} = t$), second- ($t_{\mathbf{ij}} = t'$), and third- ($t_{\mathbf{ij}} = t''$) neighbor hoppings, $a_{\mathbf{i}}$ is the phonon anihilation operator, and $n_{\mathbf{i}} = \Sigma_s n_{\mathbf{i},s}$. The third term represents the electron-phonon coupling $g = \sqrt{8\lambda\omega_0 t}$, where λ is the dimensionless EP coupling constant, and the last term represents the energy of dispersionless Einstein-type phonons ω_0. In this paper, we consider TJH model ($t' = t'' = 0$) as well as more realistic *t-t′-t″-J*-Holstein models. We simulate doped hole cuprates by choosing $t'/t = -0.34$ and $t''/t = 0.23$, which define TJHH model. Using a particle-hole symmetry operation ($t \to -t$), we obtain TJHE model, relevant for electron-doped cuprates.[16–18]

To calculate the spectral function $A_{\mathbf{k}}(\omega)$ in an undoped system, we solve Hamiltonian [Eq. (1)] for the case of one hole in an infinite two-dimensional AFM lattice. We extend the recently developed method based on the exact diagonalization within the limited functional space (EDLFS)[15] to include phonon degrees of freedom. Since details of the method have been published elsewhere,[15,19] we here only briefly discuss crucial steps. We construct the limited functional space (LFS) starting from a Néel state with one hole

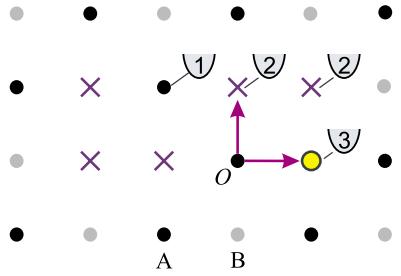

FIG. 1. (Color online) Schematic representation of a particular basis wave function obtained using $N_h=10$, $M=3$, and $N_b=3$. Circle represents the hole position, crosses portray spin flips, and numbers indicate excited phonon quanta. Dots represent lattice sites with no spin flips. Black (gray) dots represent sites on A (B) sublattice. In this particular case, $N_{fl}=5$ and $N_p=4$. Presented basis function is one of a total of $N_{st}=42\times10^6$ states, generated using Eq. (2) and parameters, given above.

with a momentum $\mathbf{k}$ and zero phonon degrees of freedom $|\phi_{\mathbf{k}}^{(0)}\rangle=c_{\mathbf{k}}|\text{Néel};0\rangle$, and proceed with generation of new states, using the following generator:

$$\{|\phi_{\mathbf{k}l}^{(N_h,M)}\rangle\}=(H_t+H_g^M)^{N_h}|\phi_{\mathbf{k}}^{(0)}\rangle, \tag{2}$$

where H_t is the hopping to nearest neighbor sites and H_g is the third term in Eq. (1). This procedure generates strings with maximum lengths given by N_h and excited phonon states at a maximal distance N_h-1 from the hole position. Parameter M provides generation of additional phonon quanta leading to a maximum number of excited phonon quanta $N_{ph}=MN_h$. Large N_{ph} is necessary to achieve convergence in the strong-coupling (SC) regime. Taking explicitly into account the translation symmetry, basis wave functions are represented by the position of the hole, by sets of strings, representing overturned spins with respect to a chosen Néel background, also referred as spin flips, and occupation numbers, representing excited phonon quanta,

$$|\phi\rangle=|\mathbf{r}_e;\mathbf{r}_1,\mathbf{r}_2,\ldots,\mathbf{r}_{N_{fl}};n_{\mathbf{r}_1'},n_{\mathbf{r}_2'},\ldots,n_{\mathbf{r}_{N_p}'},\rangle, \tag{3}$$

where $\mathbf{r}_e$ represents the hole position, $\mathbf{r}_i$ positions of spin flips, and $n_{\mathbf{r}_j'}$ occupation numbers as well as positions of phonon excitations. $N_{fl}\leqslant N_h$ represents the number of spin flips and N_p the number of excited quantum oscillators. The basis wave function is entirely defined with positions of the hole, spin flips, as well as nonzero phonon excitations. Due to broken translation invariance in a Néel state, there are two nonequivalent hole positions: the hole is located either on A or on B sublattice. The parent wave function, representing all translation invariant wave functions, is obtained by translating the hole into the origin, $\mathbf{r}_e=(0,0)$, when it is located on sublattice A or into the neighboring site, $\mathbf{r}_e=(1,0)$ (as in the case of Fig. 1), when it is located on sublattice B. Since the z component of the total spin is a conserved quantity, the number of flips N_{fl} is even, when hole is on sublattice A, and odd otherwise. For further explanation, we refer the reader to Fig. 1 as well as the underlying figure caption.

In addition, we introduce parameter N_b that restricts generation of strings. In our procedure, we keep only those states that consist of strings that, together with the hole position, fit in a box of size $N_b\times N_b$. This additional restriction keeps the total amount of states within computationally accessible limits, while it allows generation of additional states with pairs of flips in the vicinity of the hole position. The full Hamiltonian in Eq. (1) is then diagonalized within this LFS using the standard Lanczos procedure. The efficiency of the method in case of the t-J model and stability of results against varying N_h and N_b have been shown in detail in Ref. 15. The convergence of the method in terms of phonon degrees of freedom can be achieved by increasing M. More details are as well presented in the next chapter. We should also point out that despite the fact that strings are generated solely through hopping of the hole to neighboring sites, the procedure generates besides connected as well disconnected graphs. A disconnected graph is generated as the hole crosses its own path. We have checked the stability of static as well as dynamic properties of the generalized t-J-Holstein model against different basis generators. One such example can be written as

$$\{|\phi_{\mathbf{k}l}^{(N_h,M)}\rangle\}=(H_t+\tilde{H}_{J_\perp}+H_g^M)^{N_h}|\phi_{\mathbf{k}}^{(0)}\rangle, \tag{4}$$

where $\tilde{H}_{J_\perp}$ consists of only one part of the off-diagonal term representing the spin-spin interaction in Eq. (1) that erases already generated neighboring pairs of spin flips. This term generates basis states with additional disconnected paths. Using alternative generator, we found only small, physically irrelevant differences in numerical results of static as well as dynamic properties of models under investigation. All results presented in this work were obtained using the basis generator, as defined in Eq. (2).

In comparison to the alternative DMC method of Ref. 4, our method treats spin and lattice degrees of freedom on equal footing. It also enables a direct calculation of the dynamic response functions while DMC has to rely on ill-posed analytic continuation to obtain spectral properties from the imaginary-time Green function.

III. QUASIPARTICLE PROPERTIES

In Fig. 2, we present the QP weight,

$$Z_{\mathbf{k}}=|\langle\Psi_{\mathbf{k},0}^{1h}|c_{\mathbf{k}}|\Psi^{0h}\rangle|^2, \tag{5}$$

where $\Psi_{\mathbf{k},0}^{1h}$ (Ψ^{0h}) represent the ground state of the system with one (zero) hole. Note that the ground state Ψ^{0h} is a state with zero phonon quanta. A common feature to all models is ω_0-independent linear decrease of $Z_{\mathbf{k}}$ with increasing λ, characteristic for weak-coupling regime in two dimension. This result is also consistent with small-λ perturbation result.[3] EDLFS also captures the crossover λ_c to the SC limit, where the hole is localized due to lattice effects leading to vanishing $Z_{\mathbf{k}}$. With decreasing ω_0/t, the crossover becomes more pronounced and λ_c decreases. In comparison to TJH, the crossover in TJHH is, for small ω_0/t, more abrupt while λ_c increases, consistent with prediction of Ref. 5. Similar comparison is established between TJHH and TJHE. The inset of

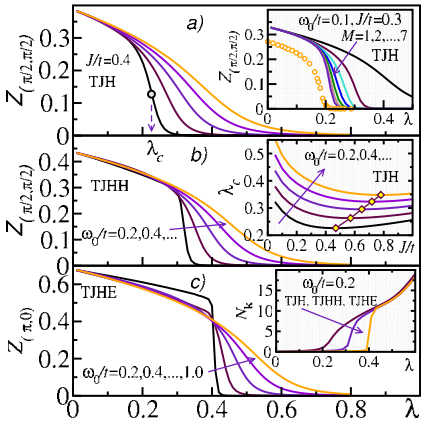

FIG. 2. (Color online) QP weight $Z_{\mathbf{k}=(\pi/2,\pi/2)}$ vs λ at different values of ω_0/t for (a) TJH, (b)TJHH, and (c) TJHE. The circle in (a) represents inflection point defining λ_c. The inset in (a) represents $Z_{(\pi/2,\pi/2)}$ vs λ for $J/t=0.3$, $\omega_0/t=0.1$, and different values of M. Circles are data taken from Ref. 4. The inset in (b) shows λ_c for the TJH model with diamonds presenting minimal values of $\lambda_c(J/t)$ at fixed ω_0/t, and the inset in (c) $N_{\mathbf{k}}$ vs λ for TJH, TJHH, and TJHE at $\omega_0/t=0.2$. In this and all subsequent figures [except in (a)], we used $J/t=0.4$, $N_h=8$, $N_b=3$, $M=7$, and $N_{st}\sim 8.1\times 10^6$. Values of t'/t and t''/t in (b) and (c) are given in the text.

Fig. 2(c) presents average phonon numbers $N_{\mathbf{k}}=\langle\Psi^{1h}_{\mathbf{k},0}|\Sigma_i a_i^\dagger a_i|\Psi^{1h}_{\mathbf{k},0}\rangle$, computed at respective band minima, for the three different models where the trend of narrowing crossover is clearly seen. Due to localization, $N_{\mathbf{k}}$ is nearly identical for all models in the SC regime. Convergence of EDLFS results in the SC regime can be verified from the inset of Fig. 2(a), where $Z_{\mathbf{k}}$ is presented for different values of M along with the results from Ref. 4.

The inset of Fig. 2(b) displays λ_c, defined with $\partial^2 Z_{(\pi/2,\pi/2)}(\lambda_c)/\partial\lambda^2=0$ vs J/t for TJH model with different values of ω_0/t. We observe a nonmonotonous dependence of $\lambda_c(J/t)$ where the shallow minima shift toward larger λ_c and J/t as ω_0/t increases.

In Fig. 3, we compare QP energies $E_{\mathbf{k}}=E^{1h}_{\mathbf{k}}-E^{0h}$ and QP weights along with $N_{\mathbf{k}}$ for all three systems, TJH, TJHH, and TJHE, as functions of wave vectors within the reduced AFM Brillouin zone (BZ). Expected common features of all models are (a) flattening $E_{\mathbf{k}}$, (b) vanishing $Z_{\mathbf{k}}$, and (c) increasing $N_{\mathbf{k}}$ with increasing λ. The energy minimum for TJH and TJHH models is, for all values of λ, at $\mathbf{k}=(\pi/2,\pi/2)$ or M point, while that for TJHE at $\mathbf{k}=(\pi,0)$ or X point, which is for $\lambda=0$, also consistent with previous works on small lattices.[16–18] Besides prominently different energy dispersions around M point, TJH and TJHH models display substantially different values of $Z_{\mathbf{k}}$, as seen from Figs. 3(b) and 3(e). While in both models $Z_{\mathbf{k}}$ reaches its maximum values somewhere on the Γ-X line, in the TJHH model, $Z_{\mathbf{k}}$ shows more pronounced $\mathbf{k}$ dependence. In the case of TJHE, $Z_{\mathbf{k}}$ peaks at X point and reaches much larger value of $Z_X\sim 0.7$, consistent with Ref. 20. Increasing λ leads to decrease of $Z_{\mathbf{k}}$ in all cases, however, the rate of decrease differs substantially between different models. While in the case of TJH model, Z_M decreases to approximately 1/2 of its original value at $\lambda=0.2$, in the case of TJHH and TJHE, the decrease

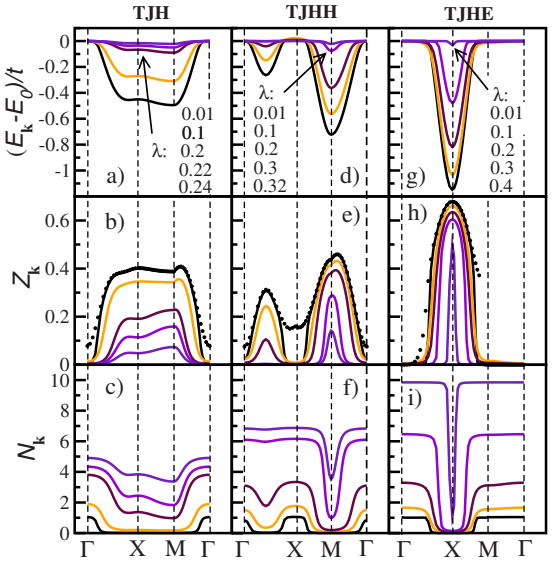

FIG. 3. (Color online) [(a), (d), and (g)] Single-hole energies $E_{\mathbf{k}}$, [(b), (e), and (h)] QP weights $Z_{\mathbf{k}}$, and [(c), (f), and (i)] average number of phonon quanta $N_{\mathbf{k}}$ for TJH, TJHH, and TJHE, respectively, presented as scans over the AFM BZ and different values of λ. Dots in (b), (e), and (h) represent results of respective t-J models with no phonon degrees of freedom. We have set $\omega_0/t=0.2$.

of $Z_{\mathbf{k}}$ from their maximum values at $\lambda=0.2$ is less than 20%. This behavior is consistent with the λ and $\mathbf{k}$ dependences of $N_{\mathbf{k}}$. With increasing λ, N_M and N_X for TJHH and TJHE models, respectively, remain small up to $\lambda\sim 0.3$ [Figs. 3(f) and 3(i)].

IV. SPECTRAL PROPERTIES

We proceed with presenting results of the hole *spectral function* $A_{\mathbf{k}}(\omega)$, directly related to ARPES spectra for undoped cuprates, calculated for TJH and TJHH models. We define $A_{\mathbf{k}}(\omega)$ as

$$A_{\mathbf{k}}(\omega)=\sum_n |\langle\Psi^{1h}_{\mathbf{k},n}|c_{\mathbf{k}}|\Psi^{0h}\rangle|^2\delta[\omega-(E^{1h}_{\mathbf{k},n}-E^{0h})], \qquad (6)$$

where $|\Psi^{1h}_{\mathbf{k},n}\rangle$ and $E^{1h}_{\mathbf{k},n}$ represent excited states and energies of the one-hole system. In Fig. 4, we first present evolution of spectral functions of the TJH and TJHH models with increasing electron-phonon coupling λ. Concentrating first on the M point [see Figs. 3(a) and 3(d)], we observe in both models a slight shift of the low-energy peak toward lower ω with increasing λ. With circles, we present positions of QP peaks that with increasing λ shift below the low-energy peaks. This shift is followed by the decrease of $Z_{\mathbf{k}}$ [see also Figs. 2(a) and 2(b)]. With increasing λ, the QP peak transforms into a broader incoherent peak that roughly preserves the spectral weight of the QP peak at $\lambda=0$, as indicated by dark-shaded areas in Fig. 4. These results are in agreement with Ref. 4. Comparison between the two models (TJH and TJHH) reveals that the low-energy peak in the strong-coupling regime remains sharper in the TJHH model at comparable values of λ. Moving to other points in the AFM BZ (X and Γ), we

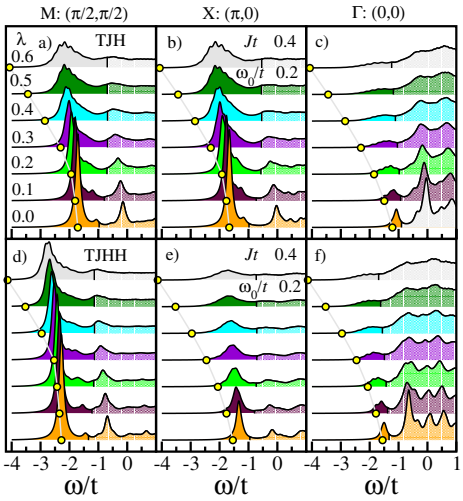

FIG. 4. (Color online) Spectral function $A_{\mathbf{k}}(\omega)$ for different values of λ. (a), (b), and (c) represent $A_{\mathbf{k}}(\omega)$ of the TJH model at M, X, and Γ points, respectively; (d), (e), and (f) represent $A_{\mathbf{k}}(\omega)$ of the TJHH model at M, X, and Γ points, respectively. Darker areas are proportional to the respective $Z_{\mathbf{k}}$ at $\lambda=0$; circles represent positions of QP peaks. In this and all subsequent figures, we have used artificial broadening $\epsilon=0.1t$.

realize that the evolution of the QP peak from coherent in the weak-coupling regime to incoherent in the strong-coupling regime with approximately conserving spectral weight is a universal feature, independent of the position in the AFM BZ.

In Fig. 5, we present sweeps of $A_{\mathbf{k}}(\omega)$ in the strong-coupling regime for TJH and TJHH models. Focusing first on the $M\rightarrow\Gamma$ sweep, we find the following experimentally most relevant features: (a) low-energy incoherent peaks disperse along $M\rightarrow\Gamma$. Dispersion qualitatively tracks the dispersion of respective t-t'-t''-J models yielding effective

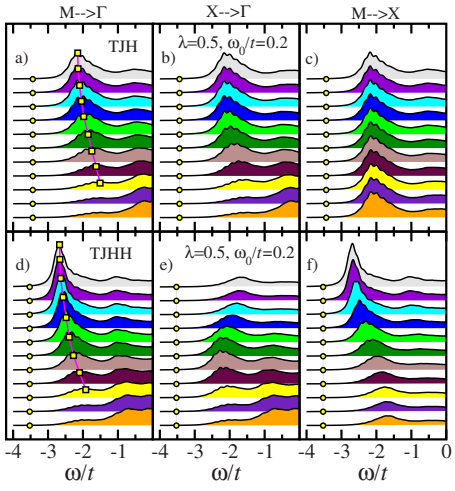

FIG. 5. (Color online) Various sweeps of spectral functions $A_{\mathbf{k}}(\omega)$ in the strong-coupling regime, $\lambda=0.5$ and $\omega_0/t=0.2$. (a)–(c) represent sweeps as indicated in respective figures (from top to bottom) of $A_{\mathbf{k}}(\omega)$ for the TJH model and (d)–(f) for the TJHH model. Circles represent positions of the QP peaks; squares are guides for the eyes emphasizing dispersion.

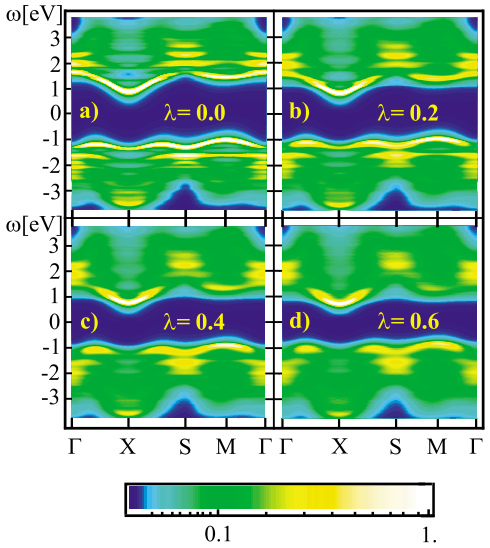

FIG. 6. (Color online) Intensity plots of $A_{\mathbf{k}}(\omega)$ for the TJHH and TJHE models along high-symmetry points of the first BZ at different values of λ. For the calculation, we have chosen identical parameters as used in Fig. 3, apart for the choice of λ. To set the energy scale, we have used $t=0.375$ meV. To obtain the $\omega>0$ part (inverse-photoemission spectra), we have used the particle-hole transformation. The on-site Coulomb interaction determining the size of the Mott gap is set to $U/|t|=4|t|/J=10$. The chemical potential is located at zero frequency. The symbol S stands for $\mathbf{k}=(\pi,\pi)$.

bandwidths $W_{\mathrm{TJH}}/t\sim0.64$ and $W_{\mathrm{TJHH}}/t\sim0.75$; (b) widths of low-energy peaks at M point are comparable to respective bandwidths, $\Gamma_{\mathrm{TJH}}/t\sim0.82$ and $\Gamma_{\mathrm{TJHH}}/t\sim0.52$; and (c) peak widths increase with increasing binding energy ($M\rightarrow\Gamma$). These effects are even more evident in the TJHH case. Positions of QP peaks, as indicated with circles, show almost no dispersion, they appear deep in the tails of spectral functions, located at $\Delta_{\mathrm{TJH}}/t\sim1.30$ and $\Delta_{\mathrm{TJHH}}/t\sim0.85$ below the low-energy peaks at M point. These observations are in quantitative agreement with ARPES data.[1] Other sweeps, presented in Figs. 5(b), 5(c), 5(e), and 5(f) as well, show dispersion, characteristic for respective models at $\lambda=0$. Latter figures also show most prominent differences between TJH and TJHH models: (a) the sweep $X\rightarrow\Gamma$ of the TJHH model shows more pronounced dispersion and a buildup of the low-energy incoherent peak around $\mathbf{k}=(\pi/2,0)$; (b) the sweep $M\rightarrow X$ of the TJHH model as well shows stronger dispersion in comparison to TJH model and a diminishing spectral weight of the incoherent low-energy peak on the approach to Γ point.

It is well know that the Hubbard model, relevant for the description of CuO_2 planes, can be in the strong-coupling limit simulated using the t-t'-t''-J model with appropriate set of parameters.[16] In Fig. 6, we present intensity plot of $A_{\mathbf{k}}(\omega)$ for the t-t'-t''-J-Holstein model. Spectral density as relevant for the photoemission as well as the inverse-photoemission experiments was calculated using the TJHH as well as the TJHE model by invoking the particle-hole transformation. We scan the first BZ along the high-symmetry lines for various values of EP coupling λ. The on-site Coulomb interac-

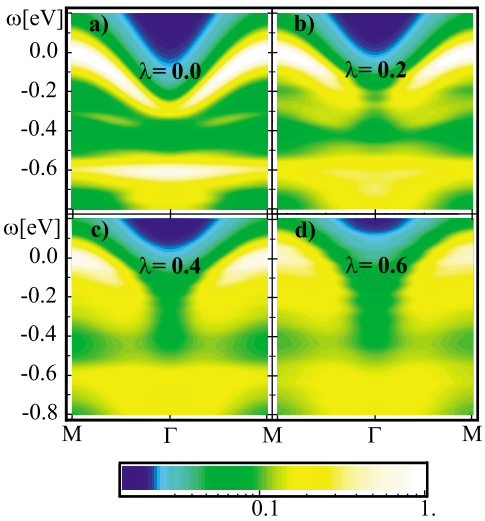

FIG. 7. (Color online) Intensity plots of $A_{\mathbf{k}}(\omega)$ for the TJHH model at different values of λ and $\omega_0/t=0.2$. To set the energy scale, we have used $t=0.375$ meV. Zero energy is set at the peak value of $A_M(\omega)$. To facilitate comparison with experiment, we transformed $\omega \rightarrow -\omega$.

tion determining the size of the Mott gap is set to $U/|t| = 4|t|/J=10$. The chemical potential is located at zero frequency. At $\lambda=0$ [Fig. 5(a)], our results match the spectra obtained using exact diagonalization technique on a $N=20$ site square lattice.[16] The maximum of the lower Hubbard band is at M point, while the minimum of the upper Hubbard band is at X point. We find the largest QP weight around the minimum of the upper Hubbard band (X point). This result indicates that the electron doped in the upper band is more coherent than the hole doped in the lower band. The QP weight at X point for the electron doped in the upper Hubbard band is around $Z_X \sim 0.7$, while its counterpart value, relevant for the hole-doped case, is much smaller, i.e., $Z_M \sim 0.4$. This effect is consistent with the asymmetry between electron vs hole-doped cuprates. More coherent electron propagation generates less scattering of a propagating electron on magnetic excitations, which is in agreement with the experimental evidence where AFM state persists up to higher electron doping. Moreover, as a consequence of the asymmetry in the spectral properties, there exists also the asymmetry in the effect of the EP coupling. Increasing of EP coupling affects less doped correlated electron at X point than the doped hole in the M point. Increasing EP coupling as well leads to slowly closing of the indirect band gap. This rather small effect is more clearly seen in Fig. 3(a) where a slight shift of the low-energy peak at M point for the hole-doped case is observed.

To investigate the possible origin of the waterfall structure as seen in underdoped cuprates,[2] we present in Fig. 7 a blow up of the intensity plot of $A_{\mathbf{k}}(\omega)$ of the TJHH model around the top of the lower band along the nodal direction. At $\lambda=0$, a dispersive low-energy QP peak with total dispersion $\Delta\omega \sim 0.3$ eV is clearly seen. The width of this peak is set by the artificial broadening $\epsilon=0.04$ eV. QP peak can be followed all the way through Γ point. The high-binding energy dispersionless feature at $\omega_1 \sim -0.6$ eV is interpreted as a string state. At rather small value of $\lambda=0.2$, the signature of the QP in the vicinity of Γ point vanishes, while the rest of the low-energy excitation broadens and remains dispersive, while the high-binding energy feature broadens. In the strong-coupling regime, $\lambda=0.4$ and 0.6, the qualitative behavior changes since the dispersion seems to transform in a single band with a waterfall-like feature at $\mathbf{k} \sim (\pi/4, \pi/4)$, connecting the low energy with the high-energy parts of the spectra. Ripples due to phonon excitations as well become visible.

V. SUMMARY

In conclusion, we have presented a numerical approach for calculating physical properties of a spin-lattice polaron. The presented method is highly efficient, while finite-size effects are well under control. The method is not model specific and can be generalized to analogous models of strongly correlated electrons.

Most relevant results can be summarized as follows. (a) We find that $Z_{\mathbf{k}}$ in the band minimum is much larger in the electron-doped than in the hole-doped case in part due to stronger antiferromagnetic correlations. Larger $Z_{\mathbf{k}}$ indicates that the QP is much more coherent and has smaller effective mass in the electron-doped case which leads to less effective EP coupling, and higher λ is required to enter the small-polaron (localized) regime; (b) spectral functions in the SC regime of the TJH as well as TJHH models are consistent with ARPES data.[1] We found that low-energy peaks are broadened due to EP coupling; their peak widths are comparable in energy to the entire bandwidths and their widths increase with binding energy. Dispersion of low-energy peaks along different cuts in the AFM BZ as well as their weights are consistent with respective dispersions and QP weights at $\lambda=0$; (c) even a weak EP coupling causes vanishing of the QP spectral weight near Γ point in the hole-doped case. The SC spectra with a waterfall resemble to a large extent the experimentally measured ARPES in undoped cuprates.[2] This could serve as another indication that excitations in undoped (as well as in low-doped) cuprates are indeed in the SC regime with respect to phonons.[5] Anomalous spectral features originate in lattice excitations of the composite spin-lattice polaron. Experimental observation of ripples would confirm that optical phonons are indeed causing anomalous spectral properties found in ARPES experiments as long as their dispersion remains much smaller than ω_0.

ACKNOWLEDGMENTS

J.B. acknowledges stimulating discussions with C. D. Batista, A. Ramšak, and I. Sega and the financial support of the SRA under Grant No. P1-0044. S.M. and T.T. acknowledge the financial support of the Next Generation Super Computing Project of Nanoscience Program, CREST, and Grant-in-Aid for Scientific Research from MEXT.

[1] K. M. Shen, F. Ronning, D. H. Lu, W. S. Lee, N. J. C. Ingle, W. Meevasana, F. Baumberger, A. Damascelli, N. P. Armitage, L. L. Miller *et al.*, Phys. Rev. Lett. **93**, 267002 (2004).
[2] F. Ronning, K. M. Shen, N. P. Armitage, A. Damascelli, D. H. Lu, Z.-X. Shen, L. L. Miller, and C. Kim, Phys. Rev. B **71**, 094518 (2005).
[3] A. Ramšak, P. Horsch, and P. Fulde, Phys. Rev. B **46**, 14305 (1992).
[4] A. S. Mishchenko and N. Nagaosa, Phys. Rev. Lett. **93**, 036402 (2004).
[5] O. Rösch, O. Gunnarsson, X. J. Zhou, T. Yoshida, T. Sasagawa, A. Fujimori, Z. Hussain, Z.-X. Shen, and S. Uchida, Phys. Rev. Lett. **95**, 227002 (2005).
[6] W. Meevasana, N. J. C. Ingle, D. H. Lu, J. R. Shi, F. Baumberger, K. M. Shen, W. S. Lee, T. Cuk, H. Eisaki, T. P. Devereaux *et al.*, Phys. Rev. Lett. **96**, 157003 (2006).
[7] X. J. Zhou, J. Shi, T. Yoshida, T. Cuk, W. L. Yang, V. Brouet, J. Nakamura, N. Mannella, S. Komiya, Y. Ando *et al.*, Phys. Rev. Lett. **95**, 117001 (2005).
[8] G.-H. Gweon, T. Sasagawa, S. Zhou, J. Graf, H. Takagi, D.-H. Lee, and A. Lanzara, Nature (London) **430**, 187 (2004).
[9] X. J. Zhou, T. Yoshida, A. Lanzara, P. V. Bogdanov, S. A. Kellar, K. M. Shen, W. L. Yang, F. Ronning, T. Sasagawa, T. Kakeshita *et al.*, Nature (London) **423**, 398 (2003).
[10] A. Alexandrov and N. F. Mott, Rep. Prog. Phys. **57**, 1197 (1994).
[11] P. Prelovšek, R. Zeyher, and P. Horsch, Phys. Rev. Lett. **96**, 086402 (2006).
[12] O. Rösch and O. Gunnarsson, Eur. Phys. J. B **43**, 11 (2006).
[13] G. Sangiovanni, O. Gunnarsson, E. Koch, C. Castellani, and M. Capone, Phys. Rev. Lett. **97**, 046404 (2006).
[14] A. Macridin, B. Moritz, M. Jarrell, and T. Maier, Phys. Rev. Lett. **97**, 056402 (2006).
[15] J. Bonča, S. Maekawa, and T. Tohyama, Phys. Rev. B **76**, 035121 (2007).
[16] T. Tohyama, Phys. Rev. B **70**, 174517 (2004).
[17] T. Tohyama and S. Maekawa, Phys. Rev. B **64**, 212505 (2001).
[18] T. Tohyama and S. Maekawa, Phys. Rev. B **67**, 092509 (2003).
[19] J. Bonča, S. A. Trugman, and I. Batistić, Phys. Rev. B **60**, 1633 (1999).
[20] C. Kim, P. J. White, Z.-X. Shen, T. Tohyama, Y. Shibata, S. Maekawa, B. O. Wells, Y. J. Kim, R. J. Birgeneau, and M. A. Kastner, Phys. Rev. Lett. **80**, 4245 (1998).